We are IntechOpen,
the world's leading publisher of
Open Access books
Built by scientists, for scientists

6,900
Open access books available

186,000
International authors and editors

200M
Downloads

154
Countries delivered to

Our authors are among the

TOP 1%
most cited scientists

12.2%
Contributors from top 500 universities

CLARIVATE ANALYTICS

BOOK CITATION INDEX

INDEXED

WEB OF SCIENCE™

Selection of our books indexed in the Book Citation Index
in Web of Science™ Core Collection (BKCI)

Interested in publishing with us?
Contact book.department@intechopen.com

Numbers displayed above are based on latest data collected.
For more information visit www.intechopen.com

Simulating Bone Atrophy and Its Effects on the Structure and Stability of the Trabecular Bone

Christoph Räth et al.[*]
Max-Planck-Institut für extraterrestrische Physik, Garching,
Germany

1. Introduction

According to the world health organization (WHO) osteoporosis is considered to belong to the ten most important diseases worldwide. It is defined as a skeletal disorder characterized by compromised bone strength predisposing to an increased risk of fracture (NIH, 2000). Osteoporosis is a metabolic bone disorder in which bones become brittle and prone to fracture. The underlying reason for the occurrence of osteoporosis is that the two processes being responsible for bone remodelling turn out of balance. Bone tissue is continuously resorbed by special bone cells, the so-called osteoclasts. On the other hand, the formation of bone also takes place by the action of other bone cells, namely the osteoblasts. These cells form new bone. The bone formation is, however, not uniform. It is rather controlled by an external mechanical stimulus such that more bone material is produced at those sites where the local stress is larger. This leads to an adaptation of the inner bone structure (trabecular bone) to externally acting forces on the bone (Mullender & Huiskes, 1995). Thereby, a minimal-weight structure, that is adapted to its applied stresses, is formed as it was already correctly conjectured by Julius Wolff as early as in 1892 (Wolff, 1892). In a healthy bone there exists an equilibrium between bone formation and bone resorption, whereas in an osteoporotic bone more bone resorption than formation takes place, which leads to a rarefied network of the trabecular bone. Besides this disease induced effect the rarefication of the inner bone structure can also have other causes like living under zero gravity conditions, immobility or age-related atrophy as the most common example.

Advances in modern imaging modalities like high resolution magnetic resonance (HRMR) or micro computed tomography (µCT) imaging have led to great improvements of the image quality especially in terms of spatial resolution which now allows for a proper three-dimensional visualisation of the trabecular network. Having these highly resolved data at

---

[*] Irina Sidorenko[1], Roberto Monetti[1], Jan Bauer[2], Thomas Baum[2], Maiko Matsuura[3],
Philippe Zysset[4] and Felix Eckstein[5]
[1]*Max-Planck-Institut für extraterrestrische Physik, Garching, Germany*
[2]*Institut für Roentgendiagnostik, Technische Universität München, Munich, Germany*
[3]*Institute of Anatomy, Ludwig Maximilians Universität München, Munich, Germany*
[4]*Institute for Lightweight Design and Structural Biomechanics,*
Vienna Universit of Technolgy (TU Wien), Wien, Austria
[5]*Institute of Anatomy and Musculoskeletal Research, Paracelsus Private Medical University, Salzburg, Austria*

hand it now becomes possible to perform a differential analysis of both the structural and the mechanical properties of the trabecular bone.

We determine the *local* structure of the trabecular network by calculating isotropic (α) and anisotropic scaling indices ($\alpha_x, \alpha_y, \alpha_z$) (Räth et al., 2008). These measures have been proven to be able to discriminate rod- from sheet-like structures and to quantify the alignment of structures with respect to a preferential direction as e.g. given by the direction of the external force.

Another class of texture measures is given by Minkowski Functionals (Michielsen & De Raedt 2001), which - as the scaling indices – also incorporate correlation functions of higher orders and supply global morphological information about structures under study.

The calculation of the local mechanical properties, i.e. the load distribution inside bodies with high porosity and complex architecture is enabled by the use of the finite element method (FEM), which has become a standard tool in bone research.

Bone modelling and remodelling processes can be simulated by describing the action of the osteoblasts and osteoclasts by means of rate equations. The equations are nonlinear partial differential equations, which can thus only be solved numerically (Huiskes et al, 2000). As it is mostly the case in nonlinear systems the solutions depend very sensitively on the choice of parameters of the model, with which e.g. the onset of bone formation is controlled.

In this chapter we propose methods to simulate the effects of bone modelling on the structure and stability of the trabecular bone. We gradually deteriorate the trabecular structure by using some concept of cellular automata (Wolfram 1983, Wolfram 1984) to solve the rate equations numerically. Specifically, both the three space coordinates as well as the time is discretised. The bone resorption, which is described as a continuous process by the partial differential equations, is thus transformed to a consecutive removal of bone surface voxel, which is discrete in space and time. Having simulated bone modelling we then assess the effects of changes in the bone structure on both the structural and mechanical properties of the specimen.

We do not consider the details of the physiological mechanisms of the bone adaptation to mechanical loading and do not describe metabolic activity of the biological cells. Rather, we assume independent action of osteoclasts (bone resorbing cells) and osteoblats (bone forming cells), which is typical for bone modelling process leading to global morphological and topological changes. Among the large variety of bone modelling scenarios we concentrate on bone atrophy due to erosion of the bone surface by osteoblasts resorption activity and decrease of osteoblast formation activity, which is typical for the process of normal aging (often called primary osteoporosis).

This type of bone modelling can be simulated by random resorption of bone voxels at the interface between trabecular bone and bone marrow. We develop three numerical models for simulation of bone loss, which correspond to the different assumptions about age-related atrophy in male and female bones: thinning of the trabecular bone structure with and without preserving of topological connectivity and with preferential loss of aligned rod-like trabecular elements, which were previously identified by a scaling index analysis.

2. Material and methods

2.1 The data set

For our study we chose 17 specimens of young (50 < age < 70) patients with high maximum compressive strength (MCS > 70 Newton (N)) out of a data set (Räth et al., 2008) of 151 cylindrical specimens with a diameter of 8 mm and a length of 14 mm, which were

harvested from 73 thoracic and 78 lumbar human vertebrae. The resulting μCT grey-value images with isotropic spatial resolution of 26 μm were segmented using a low-pass filter by convolving the image with a Gaussian kernel with standard deviation 0.8 and support of 1 to remove noise and a fixed global threshold equal to 22% of the maximal grey value to extract the mineralised bone phase (Hildebrand et al 1999). After μCT scanning, the bone samples were cut to the length of 12 mm and tested by applying uniaxial mechanical compressive load using a servo-hydraulic machine (MTS 858 mini Bionix II, MTS Eden Prairie, USA) with a load cell of 1.5 kN. Maximum compressive strength (MCS) was determined in biomechanical experiment as the first local maximum of the force-displacement curve and used in correlation analysis as a golden standard for characterisation of bone strength (Eckstein et al., 2007). Main structural characteristics of the bone specimens are given in Table 1. The binarized 3D μCT images were used as a starting structure for the numerical simulations of the bone resorption process. Table 1 summarizes some main characteristics of the data set.

	age	BV/TV	Tb.N.	Tb.Th.	Tb.Sp.	MCS [N]
Mean value	62.2	0.13	1.10	0.15	0.87	105
Standard deviation	4.7	0.03	0.15	0.02	0.12	30

Table 1. Some characteristics of the data set: Mean and standard deviation of the age, the histomorphometric parameters bone volume *BV/TV*, trabecular number *Tb.N.*, trabecular thickness *Tb.Th.*, trabecular spacing *Tb.Sp.*, and the mechanical parameter maximum compressive strength MCS.

2.2 Structure measures
2.2.1 Minkowski functionals
Minkowski Functionals (MF) (Michielsen & de Raedt 2001) provide a global morphological and topological description of structural properties of multidimensional data. In this method binarized images are considered as a union of 3D convex bodies (voxels)

$$I = \bigcup_{i=1}^{N_{bone}} \vec{p}_i(x_i, y_i, z_i)$$

According to integral geometry an *n*-dimensional body can be completely characterized by *n+1* functionals, which evaluate both size and shape of the object. In a three-dimensional space the four functionals are represented by the volume (MF_1), surface area (MF_2), integral mean curvature (MF_3) and integral Gaussian curvature (MF_4). Minkowski Functionals are derived from the theory of convex sets and expressed as volume integral for MF_1 and surface integrals over boundary *S* of the excursion set *I* with the principal radii of curvature R_1 and R_2 for other functionals.

$$MF_1 = \int_I dV \qquad\qquad MF_3 = 1/2 \int_{\partial I} \left(\frac{1}{R_1} + \frac{1}{R_2} \right) dS$$

$$MF_2 = \int_{\partial I} dS \qquad\qquad MF_4 = \int_{\partial I} \frac{1}{R_1 R_2} dS$$

The first two functionals MF_1 and MF_2 describe morphology of the structure and coincide with morphometrical parameters bone volume and surface fractions ($MF_1 = BV/TV$ and $MF_2 = BS/TV$). The fourth integral, also known as Euler characteristic χ, characterises the topological connectivity of structures and can be expressed in terms of Betti numbers β_0 (number of connected components), β_1 (number of tunnels), β_2 (number of cavities):

$$\chi = \beta_0 - \beta_1 + \beta_2 .$$

In the case of binary images we have exactly four global characteristics, which can be used as texture measures for assessment of bone strength (Monetti et al., 2011).

2.2.2 Isotropic and anisotropic scaling indices

We calculate isotropic and anisotropic scaling indices (SIM) (Räth & Morfill 1997; Monetti et al. 2004; Müller et al. 2006; Räth et al. 2008) as measures to characterize the complex trabecular network and its degree of alignment relative to a preferential direction.

Generally, scaling indices represent one way to estimate the local scaling properties of a n-dimensional point set. Considering binarised three-dimensional μCT-images, a suitable representation of the image information as a set of three-dimensional points is given by

$$\vec{p}_i = (x_i, y_i, z_i) ,$$

i = 1, . . . , N_{bone}, where N_{bone} denotes the number of (white) bone voxels and x_i, y_i, z_i the voxel position. The three-dimensional image can now be regarded as a set of N points

$$P = \{\vec{p}_i\}, i = 1,...,N_{bone} .$$

For each (bone) voxel the logarithmic gradients

$$\alpha_i = \frac{\partial \log \rho(\vec{p}_i, r)}{\partial \log r} ,$$

which are called scaling indices, of the cumulative weighted point distribution

$$\rho(\vec{p}_i, r) = \sum_{j=1}^{N_{bone}} e^{-\left(\frac{d_{ij}}{r}\right)^n}$$

are calculated with

$$d_{ij} = \left\| \vec{p}_i - \vec{p}_j \right\|_2 = \left((x_i - x_j)^2 + (y_i - y_j)^2 + (z_i - z_j)^2 \right)^{1/2}$$

for the isotropic case.

The calculation of the scaling indices depends on the parameters n and r. The exponent n controls the shape of the weighting function. With increasing n the weighting function becomes more and more step-like. In all our studies we found that n has only little influence on the results. For the following calculations we fixed n to $n=2$, which emphasises the connection to Gaussian smoothing or kernel functions. The scale parameter r controls to which scales of the image structure the scaling indices are sensitive. From previous studies

we found that $r = 8$ (in voxel units) is a well-suited choice. By means of the scaling indices α one can then discriminate between voxels belonging to rod-like ($\alpha \cong 1$) and sheet-like ($\alpha \cong 2$) structural elements of the trabecular network, which is one of most important discriminating feature to discern healthy from osteoporotic bone structure.

It is straightforward to implement anisotropies in the calculation of the scaling indices by introducing an ellipsoidal distance measure with the eigenvalues λ_x, λ_y and λ_z:

$$d_{ij} = \left\| \vec{p}_i - \vec{p}_j \right\|_{\lambda_x, \lambda_y, \lambda_z} = \left(\lambda_x^2 (x_i - x_j)^2 + \lambda_y^2 (y_i - y_j)^2 + \lambda_z^2 (z_i - z_j)^2 \right)^{1/2}$$

In this study we calculate anisotropic scaling indices α_z with respect to the direction of the external force acting in the bone, for which we chose the ratio of 5:1 for the eigenvalues, i.e. $\lambda_z = 5\lambda_x = 5\lambda_y$, for setting the degree of anisotropy along the z-direction. This setting was found to be well suited especially for the detection of aligned cylindrical structures (i.e. the trabeculae) with typical mean breadth and length.

2.3 Finite element models

For assessing biomechanical strength of trabecular network we apply Finite Element Method (FEM) with linear elastic assumptions (Rietbergen et al., 1995; Rietbergen et al., 1999; Sidorenko et al. 2009). For the bone mineral material we assume isotropic properties with Young's modulus $Y = 10\ GPa$ and Poisson's ratio $\nu = 0.3$ and describe relationship between stress σ and strain ε components by generalized Hooke's law (constitutive equations), which states that stress is proportional to the strain up to the elastic limit

$$\sigma_{ij} = 2\mu\varepsilon_{ij} + \lambda\delta_{ij}\sum_{k=1}^{3}\varepsilon_{kk}\ .$$

Material properties are included in the model through Lame parameters λ and μ

$$\{Y, \nu\} \Rightarrow \left\{ \lambda = \frac{Y\nu}{(1+\nu)(1-2\nu)},\quad 2\mu = \frac{Y}{1+\nu} \right\}$$

We use Dirichlet boundary conditions with prescribed on the top surface constant strain $\varepsilon_0 = 1\%$ to simulate uniaxial loading in the natural direction (in this work denoted as z axis) applied in biomechanical experiment. We generate a finite element mesh by direct converting image voxels that belong to the bone tissue into equally sized and oriented eight node brick elements. An exact number of nodes depend on the structure characteristics and varies for our data set from $0.7 \cdot 10^6$ for weak bones, dominated by rod-like trabecular elements, up to $2 \cdot 10^6$ for strong bones with a lot of plate–like formations. From discrete nodal displacements obtained from FEM strain and stress components can be recovered at any point of the structure. For correlation analysis with respect to the MCS we use apparent total reaction force F_r at the top face A^t which is recalculated from the normal stress component in direction of applied mechanical load σ^t_{zz}:

$$F_r = \int \sigma^t_{zz} dA^t\ .$$

2.4 Bone resorption models

We develop three numerical models for bone resorption, which correspond to the different assumptions about bone atrophy in male and female bones. Several investigations (Aaron et al., 1987; Khosla et al., 2006) demonstrated sex difference in trabecular bone aging. Although the decrease with age in trabecular bone volume is common for both sexes, male cancellous bone exposes uniform thinning, whereas female trabecular network suffers from loss of connectivity and entire rod-like structural elements (Barger-Lux et al., 2002).

In all three models we simulate the random resorption of bone material by removal surface voxels according to the given value of relative bone loss volume $\Delta BV/TV$, but with different topological features. In order to study the role of topological connectivity for bone strength in the first resorption model (Model I), a bone voxel is removed only if does not change topology of the system, i.e. no new cavities or tunnels are created. In terms of global topological characteristics it means that the fourth Minkowski Functional, which coincides with Euler characteristic χ is conserved,

$$MF_4 = \chi = \text{const.}$$

We compare this model with two other models, which both do not preserve the connectivity ($\chi \neq const$). In Model II there isn't any limitations or conditions on the removal of bone surface voxels. In Model III, however, we simulate the preferential destruction of rod-like trabecular elements by only removing surface voxels with local topological anisotropic scaling index $\alpha_z < 2$. Typical changes in trabecular bone structure are demonstrated in Fig. 1. Three regions in circles show the differences in structure due to different resorption models: preserving of connectivity and destroying of rod-like elements at the same place in the trabecular network.

3. Results

As a main characteristic of the statistical analysis we use Pearson's correlation coefficient r_{MCS} (Tables 2 - 5) with respect to the Maximum Compressive Strength (MCS) as it was measured in biomechanical uniaxial compressive experiments. In the Figs. 2 - 4 we show the changes of the different texture measures (black curves and left axis) calculated by MF, SIM and FEM as a function of bone loss. The red curves and right axis in the Figs. 2 - 4 and the values in the corresponding Tables 2 - 4 denote Pearson's correlation coefficient r_{MCS} as function of bone loss for the three resorption models.

The diagrams for the first Minkowski Functional $MF_1 = BV/TV$ (Fig. 2, first row) confirm the linear decrease in bone mineral volume due to resorption and thus represent a validation of our implementation of the bone loss models.

Plots for $MF_4 = \chi$ (Fig. 2, last row) proof that in first resorption model (left column) the connectivity is preserved ($\chi = const$) and in the two other models the porosity of the structure increases ($\Delta\chi < 0$) during the resorption process. In both models the increase of porosity occurs due to increase of number of tunnels (β_1). In the third model with preferential resorption of rod-like trabecular elements (with $\chi \neq const$ and $\alpha_z < 2$) the growth of number of tunnels (β_1) is compensated by an increase of number of separate parts (β_0) and slows down negative increase of χ. For both resorption models without conservation of connectivity for structure with large relative bone loss ($\Delta BV/TV > 30\%$) the correlation coefficient of $MF_4 = \chi$ with MCS becomes considerably higher than that for original structure (Tables 2).

Original   χ=const

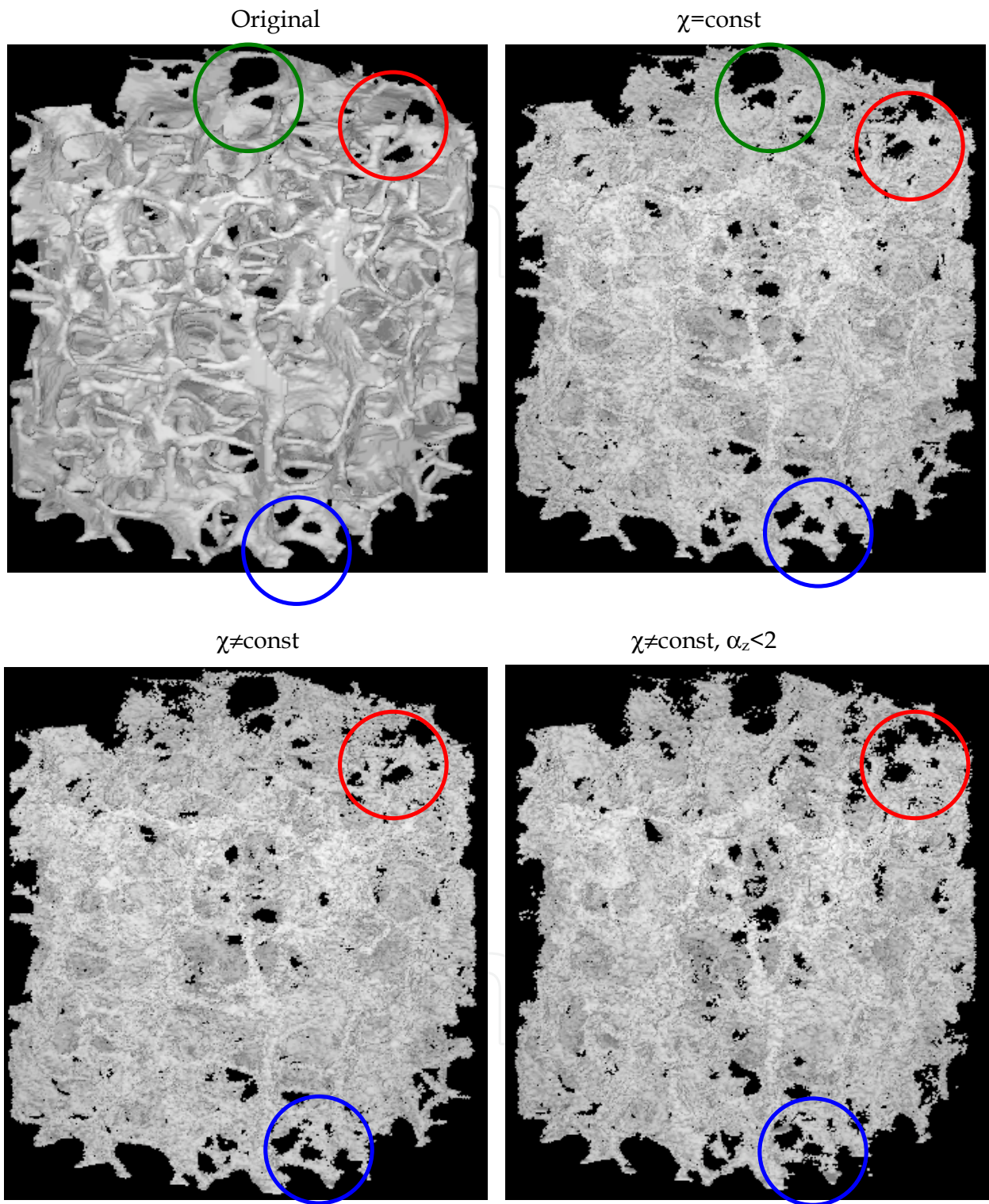χ≠const   χ≠const, $\alpha_z < 2$

Fig. 1. Typical change of the trabecular bone structure under numerically simulated bone resorption (upper left: original bone, upper right: connectivity preserving model, lower left: model without preserving connectivity, lower right: model with preferential resorption of rod-like trabecular elements).
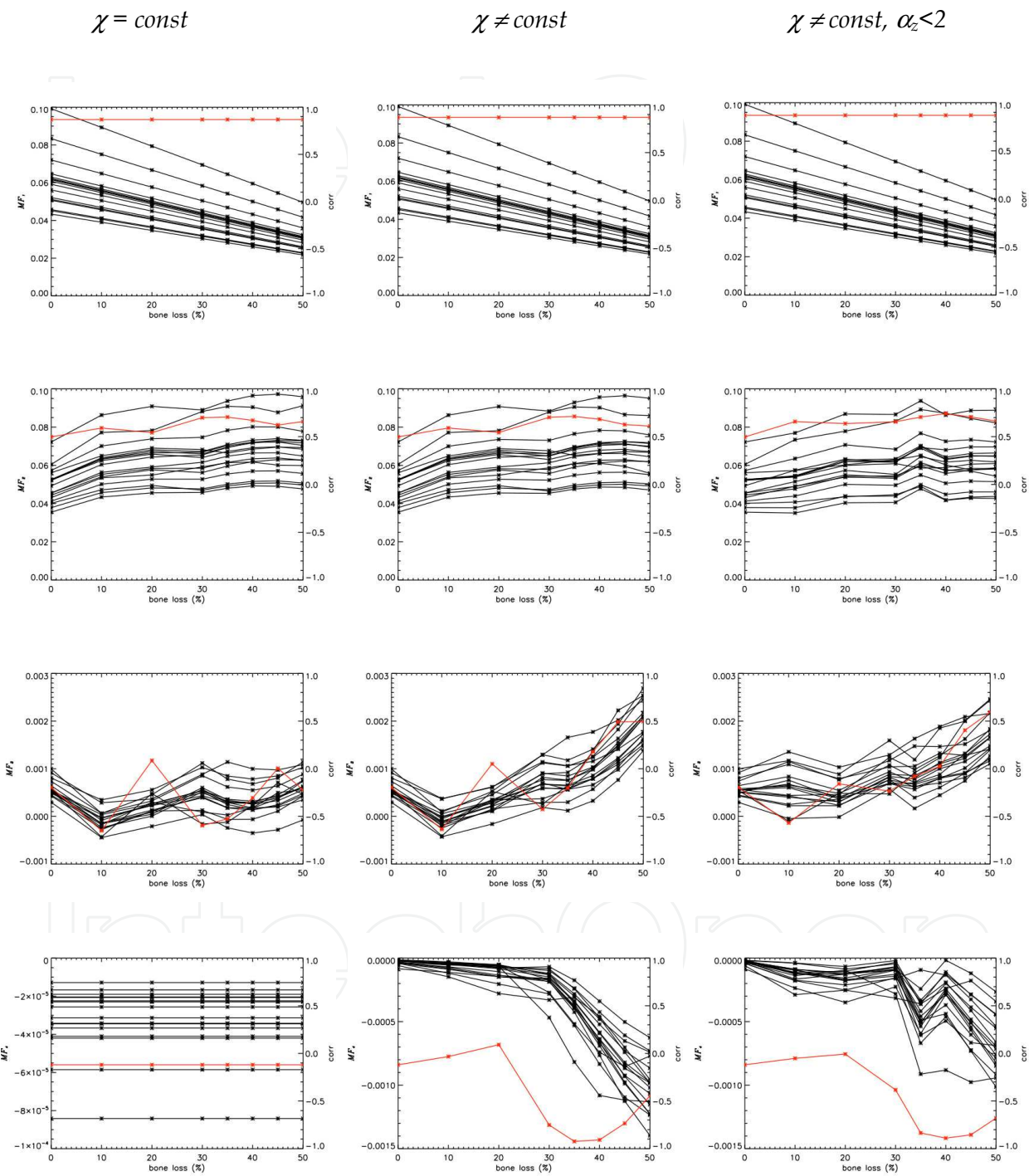
Minkowski Functionals

| $\chi = const$ | $\chi \neq const$ | $\chi \neq const, \ \alpha_z < 2$ |

Fig. 2. Minkowski Functionals for 17 specimens (black curves and left axis) and correlation coefficient with MCS (red curve and right axis) for three models of bone loss (from left to right).

Model I

	MF_1	MF_2	MF_3	MF_4
0%	0.87	0.50	-0.20	-0.12
10%	0.87	0.59	-0.65	-0.12
20%	0.87	0.54	0.09	-0.12
30%	0.87	**0.70**	-0.60	-0.12
35%	0.87	**0.71**	-0.53	-0.12
40%	0.87	0.67	-0.31	-0.12
45%	0.87	0.62	0.0	-0.12
50%	0.87	0.66	-0.22	-0.12

Model II

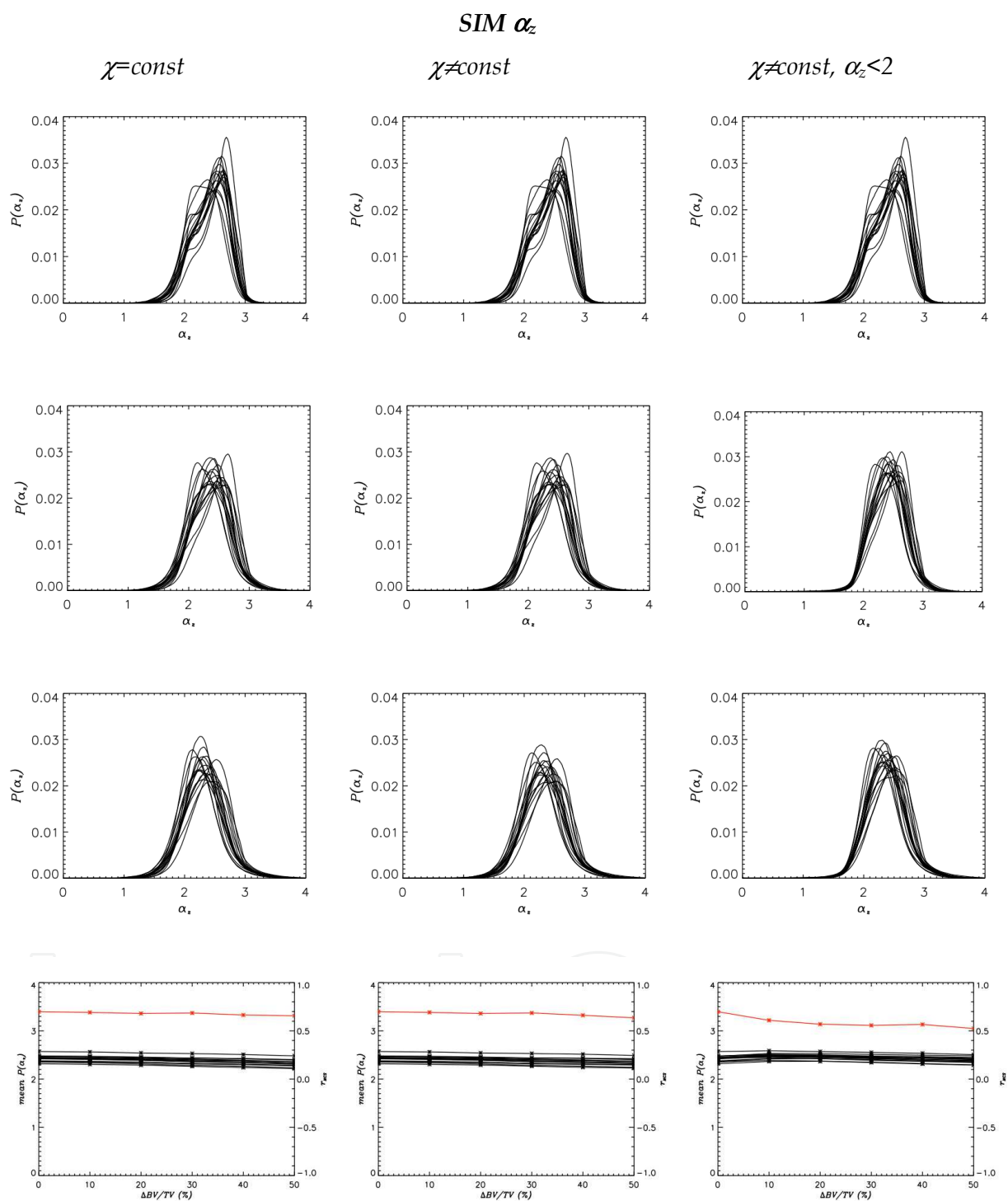|	MF_1	MF_2	MF_3	MF_4
0%	0.87	0.50	-0.20	-0.12
10%	0.87	0.59	-0.64	0.01
20%	0.87	0.54	0.05	0.09
30%	0.87	**0.70**	-0.43	**-0.75**
35%	0.87	**0.71**	-0.20	**-0.92**
40%	0.87	0.68	0.18	**-0.91**
45%	0.87	0.63	**0.49**	**-0.73**
50%	0.87	0.61	**0.50**	**-0.45**

Model III

	MF_1	MF_2	MF_3	MF_4
0%	0.87	0.50	-0.20	-0.12
10%	0.87	0.66	-0.57	-0.05
20%	0.87	0.64	-0.16	-0.01
30%	0.87	0.66	-0.25	**-0.38**
35%	0.87	**0.70**	-0.08	**-0.83**
40%	0.87	**0.74**	0.03	**-0.89**
45%	0.87	**0.71**	**0.40**	**-0.85**
50%	0.87	0.66	**0.59**	**-0.68**

Table 2. Pearson's correlation coefficient of the four MF with respect to MCS for the three models of bone loss and eight rareficiation steps ranging from 0% to 50% removal of the initial bone volume.

For isotropic SIM (Fig. 3a) there is almost no difference in the $P(\alpha)$ spectrum for the different resorption models observed, which leads to only a small decrease in the correlation coefficient (last row in Fig. 3a and Table 3a). For anisotropic SIM (Fig. 3b) there is an obvious difference in $P(\alpha_z)$ already at $\Delta BV/TV = 10\%$ and a more considerable decrease of r_{MCS} (last row on Fig.3b and Table 3b) in the case of preferential resorption of rod-like trabecular elements (third model with $\chi \neq const$ and $\alpha_z < 2$).

Fig. 3a. Probability distribution function of isotropic scaling index $P(\alpha)$ for 17 bone specimens with original structure (first row) and with different value of bone resorption (30%: second row, 50% third row). Last row: mean value of α spectrum (black curves and left axis) and correlation coefficient of mean value with MCS (red curve and right axis) for three models of bone loss (from left to right).

Fig. 3b. Probability distribution function of anisotropic scaling index $P(\alpha_z)$ for 17 bone specimens with original structure (first row) and with different value of bone resorption (30%: second row, 50% third row). Last row: mean value of α_z spectrum (black curves and left axis) and correlation coefficient of mean value with MCS (red curve and right axis) for three models of bone loss (from left to right).

	χ=const	$\chi \neq$const	$\chi \neq$const, α_z<2
0%		0.69	0.69
10%	0.67	0.67	0.64
20%	0.64	0.64	0.61
30%	0.63	0.63	0.60
40%	0.60	0.60	0.58
50%	0.57	0.56	0.55

a)

	χ=const	$\chi \neq$const	$\chi \neq$const, α_z<2
0%	0.70	0.70	0.70
10%	0.69	0.69	0.61
20%	0.68	0.68	0.57
30%	0.68	0.68	0.56
40%	0.66	0.66	0.56
50%	0.66	0.64	0.52

b)

Table 3. Correlation coefficient of mean value of α spectrum *(a)* and α_z spectrum *(b)* with MCS for three models of bone loss.

The mechanical strength of the resorbed trabecular structure as determined with FEM (Fig. 4) depends almost linearly on the relative bone loss $\Delta BV/TV$ and shows small decrease in the correlation with MCS (Table 4). At high bone loss ($\Delta BV/TV = 50\%$) the mechanical strength of all bone specimens was found to be larger in the case with conservation of connectivity (solid line in Fig. 5). In Table 5 we summarise effect of large bone loss ($\Delta BV/TV = 40\%$) on different numerical texture measures. FEM and SIM demonstrate small drop in correlation with MCS of initial structure. These methods can be proposed for prediction of osteoporosis: relative strength and local topology do not change considerably under the process of random surface resorpton. In a contrast, after large bone resorption global MF_2 and especially MF_4 improve their correlation with MCS of the original structure. This effect can be used for the diagnostic of the current state of the bone structure.
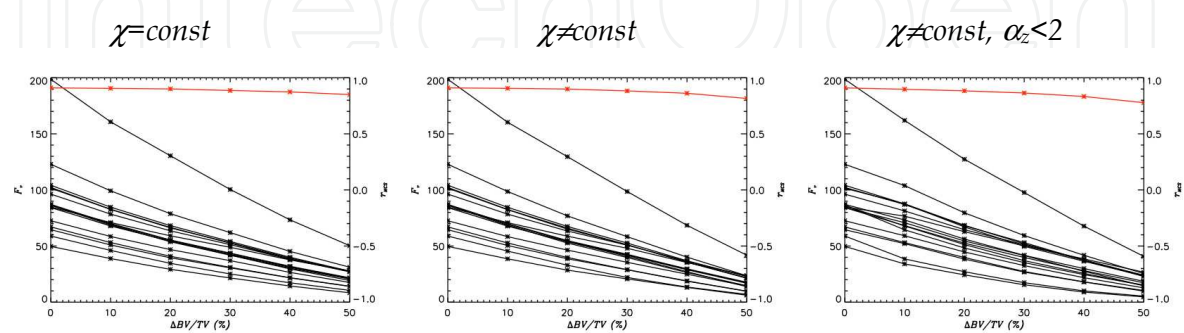

Fig. 4. Value of the apparent top reaction force F_r for 17 bone specimens calculated by FEM (black curves and left axis) and correlation coefficient of F_r with MCS (red curve and right axix) for three different resorption models (from left to right).

	χ=const	$\chi\neq$const	$\chi\neq$const, α_z<2
0%	0.91	0.91	0.91
10%	0.91	0.91	0.89
20%	0.90	0.90	0.88
30%	0.89	0.88	0.86
40%	0.87	0.86	0.83
50%	0.85	0.82	0.77

Table 4. Correlation coefficient of apparent top reaction force F_r calculated by FEM with MCS for three models of bone loss.
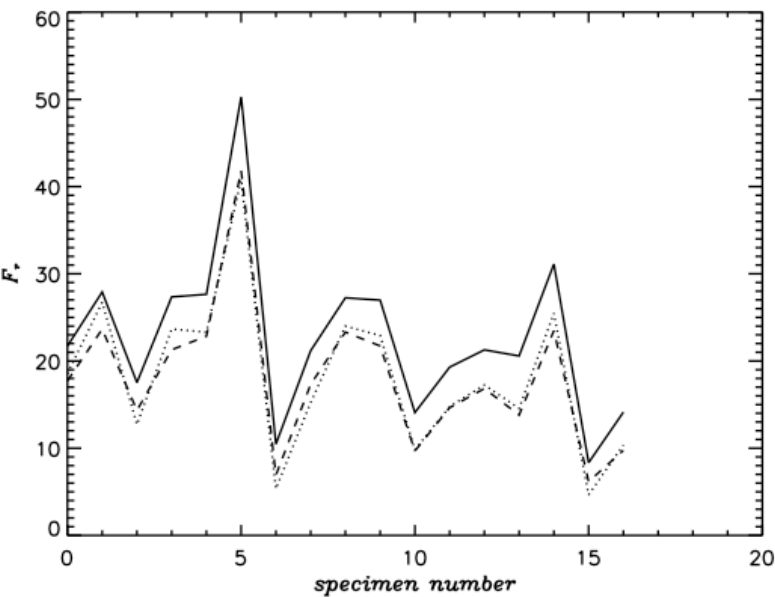

Fig. 5. Apparent total reaction force F_r for 17 bone specimens and for the three resorption models with $\Delta BV/TV$=50% (solid line: χ=const, dashed line: $\chi\neq$const, dotted line: $\chi\neq$const, α_z<2.

	original	χ=const	$\chi\neq$const	$\chi\neq$const, α_z<2
FEM	0.91	0.87	0.86	0.83
MF_1	0.87	0.87	0.87	0.87
MF_2	0.50	0.67	0.68	0.74
MF_3	-0.20	-0.31	0.18	0.03
MF_4	-0.12	-0.12	-0.91	-0.89
Mean $P(\alpha)$	0.69	0.60	0.60	0.58
Mean $P(\alpha_z)$	0.70	0.66	0.66	0.56

Table 5. Pearson's correlation coefficient with respect to the MCS for bone structure with $\Delta BV/TV$=40% for original structure and three resorption models

4. Summary and conclusions

We proposed a method based on the ideas of cellular automata to simulate bone atrophy and applied it to a sample of 17 bone probes visualised with high resolution µCT imaging. Although our study is so far restricted to the simulation of bone loss and did not include any processes of bone formation, we could already gain some new and very interesting insights about the important factors determining the strength of bones.

As expected we found that the initial structure determines the relative strength of the bone under random surface bone losses. Patients with stronger bones in young age have better prognosis for age-related bone atrophy. We found that the connectivity plays the most important role in determining the strength of the bone structure: among three resorption models the highest apparent reaction force was calculated for the resorption model which preserved the connectivity ($\chi = const$). FEM, isotropic SIM, the first and second MF yielded stable values of the correlation coefficient r_{MCS} under the random bone loss process for all numerical resorption models and can be recommended for prediction of bone strength in bone atrophy process.

The mean value of the anisotropic scaling indices α_z demonstrated sensibility for preferential rod-like trabecular loss as simulated by third numerical resorption model (with $\chi \neq const$ and $\alpha_z < 2$). For this model the scaling index approach shows a decrease of correlation coefficient r_{MCS} already at 10% loss of mineral bone fracture.

For the two resorption models without conservation of the connectivity ($\chi \neq const$) the bone surface resorption significantly improves the correlation of the fourth MF with MCS (from $r_{MCS} = -0.12$ for original structure up to the $r_{MCS} = -0.92$ for bone loss ratio $\Delta BV/TV = 35\%$). Such an effect suggests that the random surface resorption destroys thin and unimportant connections of the trabeculae and only the strong and thick trabecular elements are taken into account for correlation with MCS. The removal of bone voxels can thus be interpreted as a distillation of the essential skeleton of the trabecular structure, which is a much more sensitive tracer of the mechanical stability of the bone. In fact we found that fourth Minkowski Functional calculated for structure prepared by random surface resorption yields higher correlations with MCS than FEM-based measures, which are so far considered to yield the highest correlations with the mechanical properties of bone probes. Therefore the rarefication procedure as outlined in this study in combination with Minkowski Functionals may lead to a novel technique for the diagnosis of the trabecular bone quality and strength in the prediction of osteoporosis.
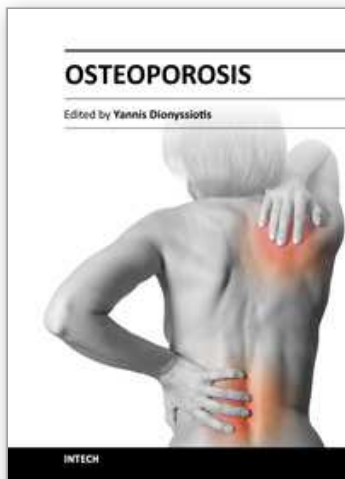
5. Acknowledgments

6. References

Aaron, J.E.; Makins, N.B. & Sagreiya, K. (1987). The Microanatomy of Trabecular Bone Loss in Normal Aging Men and Women. *Clinical Orthopaedics and Related Research*, No. 215, pp. 260-271

Barger-Lux, M.J. & Recker, R.R. (2002), Bone microstructure in osteoporosis:transilial biopsy and histomorphometry. *Topics in Magnetic Resonance Imaging,* Vol. 13, No. 5, pp. 297-306

Eckstein, F.; Matsuura M.; Kuhn, V.; Priemel, M.; Müller R.; Link, TM. & Lochmüller, EM. (2007). Sex Differences of Human Trabecular Bone Microstructure in Aging Are Site-Dependent. *J. Bone Miner. Res.* Vol. 22, No 6, pp. 817–824

Hildebrand, T.;Laib, A.; Müller, R.; Dequeker, J. & Rüegsegger, P. (1999). Direct three-dimensional morphometric analysis of human cancellous bone: microstructural data from spine, femur iliac crest, and calcaneus. *J Bone Miner Res,* Vol. 14, No. 7, pp. 1167-1174

Huiskes, R.; Ruimerman, R.; et al. (2000). Effects of mechanical forces on maintenance, adaptation of form in trabecular bone. *Nature*, Vol. 405, pp. 704-706

Khosla, S.; Riggs, B.L.; Atkinson, E.J.; Oberg, A.L.; McDaniel, L.J.; Holets, M.; Peterson, J.M. & Melton, L.J. (2006), Effects of sex and age on bone microstructure at the ultradistal radius: a population-based noninvasive in vivo assessment. *J Bone Miner Res.*, Vol. 21, No. 1, pp.124-131

Michielsen, K.; De Raedt, H. (2001). Integral-geometry morphological image analysis. *Physics Reports,* Vol.347, pp.461-538

Monetti, R.A.; Böhm, H.; Müller, D.; Rummeny, E.; Link, T. & Räth, C. (2004). Assessing the biomechanical strength of trabecular bone in vitro using 3D anisotropic non- linear texture measures: The Scaling Vector Method. *Proceedings of Medical Imaging Conference of SPIE,* Vol. 5370, pp. 215-224

Monetti, R.A.; Bauer J.; Sidorenko I.; Müller D.; Rummeny E.; Matsuura M.; Eckstein F.; Lochmueller E.-M.; Zysset P. & Räth C. (2011). Structure based classification of μ-CT images of human trabecular bone using local Minkowski Functionals. *Proceedings of Medical Imaging Conference of SPIE,* Vol. 7965 79650K

Müller, D.; Link, T.M.; Monetti, R.; Bauer, J.; Böhm, H.; Seifert-Klauss, V.; Rummeny, E.J.; Morfill, G.E. & Räth, C. (2006). The 3D-based scaling index algorithm: a new structure measure to analyze trabecular bone architecture in hifh-resolution MR images in vivo. *Osteoporos. Int.,* Vol. 17, pp. 1783-1493

Mullender, M. G.; Huiskes, R. (1995). A proposal for the regulatory mechanism of Wolff 's law. J. Orthop. Res., 13, pp. 503–512 .

NIH: National Institutes of Health (2000). NIH Consens. Statement 17, pp. 1 – 45

Räth, C. & Morfill, G. (1997). Texture detection and texture duscrimination with anisotropic scaling indices. *J. Opt. Soc. Am. A,* Vol. 14, No. 12, pp. 3208-3215

Räth, C.; Monetti, R.; Bauer, J.; Sidorenko, I.; Müller, D.; Matsuura, M.; Lochmüller, E.-M.; Zysset, P. & Eckstein, F. (2008). Strength through structure: visualization and local assessment of the trabecular bone structure. *New Journal of Physics,* Vol. 10, pp. 125010-125027

Rietbergen, B.; Weinans, H.; Huiskes, R. & Odgaard, A. (1995). A new method to determine trabecular bone elastic properties and loading using micromechanical finite-element models. *J. Bioemchanics,* Vol. 28, No. 1, pp. 69-81

Rietbergen, B.; Weinans, H. & Huiskes, R. (1996). Computational strategies for iterative solutions of large FEM applications employing voxel data, Int. J. Num. Meth. Eng. 39, pp. 2743-2767

Sidorenko, I.; Bauer, J.; Monetti, R.; Müller, D.; Rummeny, E.; Eckstein, F.; Matsuura, M.; Lochmüller, E.-M.; Zysset, P.; Räth, C. (2009). Role of trabecular microfractures in failure of human vertebrae estimated by the finite element method, Proceedings of the SPIE, 7262, pp. 72620M

Wolff, J. (1892). Das Gesetz der Transformation der Knochen, Hirschwald Verlag, Berlin.

Wolfram, S. (1983). Statistical Mechanics of Cellular Automata, Rev. Mod. Phys., 55, pp. 603-644

Wolfram S. (1984). Cellular automata as models of complexity, Nat. 311, pp. 419-424

Osteoporosis

Edited by PhD. Yannis Dionyssiotis

Osteoporosis is a public health issue worldwide. During the last few years, progress has been made concerning the knowledge of the pathophysiological mechanism of the disease. Sophisticated technologies have added important information in bone mineral density measurements and, additionally, geometrical and mechanical properties of bone. New bone indices have been developed from biochemical and hormonal measurements in order to investigate bone metabolism. Although it is clear that drugs are an essential element of the therapy, beyond medication there are other interventions in the management of the disease. Prevention of osteoporosis starts in young ages and continues during aging in order to prevent fractures associated with impaired quality of life, physical decline, mortality, and high cost for the health system. A number of different specialties are holding the scientific knowledge in osteoporosis. For this reason, we have collected papers from scientific departments all over the world for this book. The book includes up-to-date information about basics of bones, epidemiological data, diagnosis and assessment of osteoporosis, secondary osteoporosis, pediatric issues, prevention and treatment strategies, and research papers from osteoporotic fields.

INTECH
open science | open minds